

Supporting information

Molecular design and crystallization process control for thin sheet-shaped organic semiconductor crystals with two-dimensional packing

Yuejuan Wan, ‡^a Zejian Zhang, ‡^a Haichao Liu, ^c Jiadong Zhou, ^a Liqun Liu, ^a Jian Deng, ^a and Yuguang Ma* ^{ab}

^aState Key Laboratory of Luminescent Materials and Devices, Institute of Polymer Optoelectronic Materials and Devices, South China University of Technology, No. 381 Wushan Road, Tianhe District, Guangzhou 510640, P. R. China.

^bGuangdong Provincial Key Laboratory of Luminescence from Molecular Aggregates, South China University of Technology, Guangzhou 510640, P. R. China.

^cState Key Laboratory of Supramolecular Structure and Materials, College of Chemistry, Jilin University, Changchun 130012, P.R. China.

Corresponding Author

E-mail:

*yigma@scut.edu.cn.

Materials

All the target compounds were synthesized referred to literatures from our groups. N₂ (99.9999%) and Ar (99.9999%) were purchased form *Mulai* gas company.

Methods

Single-crystal X-ray diffraction (SXRD) data were recorded on an XtaLAB P200 FR-X. The powder X-ray diffraction (PXRD) data were conducted on a synchrotron X-ray and multiple PILATUS 100 K detectors of the BL5S2 beam line ($\lambda = 1.54056 \text{ \AA}$) at Aichi Synchrotron Radiation Centre. Optical images were recorded through Leica fluorescence microscope with DM4000 excitation at 340 to 380 nm. The characterization of the electrical properties of the devices was performed by the semiconductor parameter analyzer (Agilent Technologies B1500A and Keithley 2636B) in the glove box.

Crystal growth

The crystal growth procedure was conducted in a quartz tube, placed in the two-stage heating furnace. The first-stage heating temperature was named as sublimation temperature, and the second-stage temperature was termed as growth temperature. When the powder was placed at the first-stage heating source, the quartz tube was vacuumed before the argon gas flowing into the quartz tube. After a period of argon gas flow, the temperature was increased to the setting temperature. The rod- or sheet-shaped crystals were grown on the quartz tube.

Distribution of electrostatic potential (ESP)

The molecular geometries for the ground and charged states were optimized by density functional theory (DFT) at the RB3LYP/6-31G(d,p) level. Based on the optimized ground-state electron density, atomic charges were obtained and the electrostatic potentials were plotted using the GaussView package.

Morphology simulation of single crystal

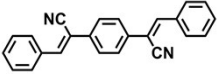
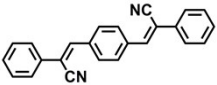
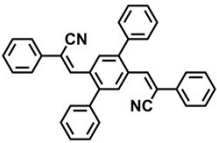
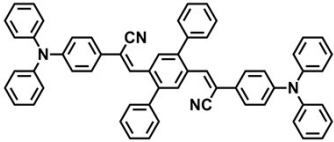
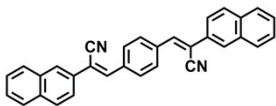
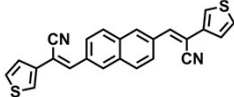
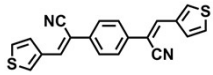
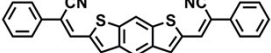
The morphologies of single crystals were simulated based on the cif files of single crystal structures. The “growth morphology” method were selected to simulate the crystal morphology and corresponding attachment energies of final facets. The attachment energy of facet is positively proportional to the growth rate of facet. The facets with higher attachment energy grow faster, disappearing with larger probability finally.

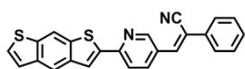
Device preparation based on the organic field-effect transistor

The highly conductive p-silicon wafers with the electrical impedance rate of 0.002 to 0.005 $\Omega \text{ mm}^{-1}$ were chosen as device substrate. The cleaned surface was modified by the polymethyl-methacrylate (PMMA) films with 80 nm. The single crystals were tightly placed on the substrate with the impact of electrostatic interaction. The calculated gate-channel capacitance per unit area (C_i) was calculated to be $1.22 \times 10^{-8} \text{ F cm}^{-2}$ based on the thickness of SiO_2 and PMMA layers. The 200-nm gold and 150-nm calcium were used as asymmetric electrodes, with 2-nm Cesium fluoride and molybdenum trioxide as the modification layers to improve the injection of electron and hole, respectively. All the electrical performance tests were conducted in the glove box.

Supporting tables

Table S1 The chemical structures of reported thin sheet-shaped organic single crystals with 2D packing from our research group.

Chemical structures	References
 <p>CN-DSB</p>	<p><i>J. Mater. Chem. C</i>, 2016, 4, 1257–1262; <i>CrystEngComm</i>, 2016, 18, 6824–6829.</p>
 <p>BCPEB (CN-DSB, β-CNDSB)</p>	<p><i>Org. Electron.</i>, 2012, 13, 762–766; <i>Phys. Chem. Chem. Phys.</i>, 2015, 17, 3421–3425; <i>Chem. Commun.</i>, 2016, 52, 2370–2373.</p>
 <p>CN-DPDSB</p>	<p><i>Appl. Phys. Lett.</i>, 2007, 90, 141110; <i>Chem. Commun.</i>, 2007, 3, 231–233; <i>Adv. Funct. Mater.</i>, 2011, 21, 3770–3777.</p>
 <p>CNDPASDB</p>	<p><i>Chem. Mater.</i>, 2008, 20, 7312–7318; <i>Appl. Phys. Lett.</i>, 2012, 101, 063301.</p>
 <p>PBNA</p>	<p><i>Faraday Discuss.</i>, 2017, 196, 415–42; <i>ACS Mater. Lett.</i>, 2021, 3, 428–432.</p>
 <p>NBTA</p>	<p><i>ACS Appl. Mater. Interfaces</i>, 2020, 12, 43976–43983.</p>
 <p>α-PBTA</p>	<p><i>Chem. Commun.</i>, 2020, 56, 13776–13779.</p>
 <p>β-DBPA</p>	



PCPyBDT

J. Mater. Chem. A, 2021, **9**, 2120–2125.

Table S2 Crystallographic data and structural refinement summary for rod- and sheet-shaped crystals.

Identification code	NBTA (sheet)	NBTA (rod)
Empirical formula	C ₂₄ H ₁₄ N ₂ S ₂	C ₂₄ H ₁₄ N ₂ S ₂
Formula weight	394.49	394.49
Temperature/K	150.00(10)	119.99(13)
Crystal system	monoclinic	monoclinic
Space group	P2 ₁ /c	P2 ₁ /c
<i>a</i> (Å)	6.95686(16)	6.9349(10)
<i>b</i> (Å)	4.79577(13)	4.7850(6)
<i>c</i> (Å)	28.1400(7)	28.129(5)
α (°)	90	90
β (°)	94.683(2)	94.652(18)
γ (°)	90	90
Volume (Å ³)	935.71(4)	930.4(2)
<i>Z</i>	2	2
ρ_{calc} (g cm ⁻³)	1.4	1.408
μ (mm ⁻¹)	2.662	2.677
<i>F</i> (000)	408	408
Crystal size (mm ³)	0.16 × 0.1 × 0.1	0.1 × 0.08 × 0.06
Radiation	CuK α (λ = 1.54184)	CuK α (λ = 1.54184)
Reflections collected	3705	3773
Independent reflections	1825 [<i>R</i> _{int} = 0.0203, <i>R</i> _{sigma} = 0.0256]	1652 [<i>R</i> _{int} = 0.0699, <i>R</i> _{sigma} = 0.0951]
Data/restraints/parameters	1825/0/127	1652/0/127
Goodness-of-fit on <i>F</i> ²	1.078	1.08
Final <i>R</i> indexes [<i>I</i> ≥ 2σ (<i>I</i>)]	<i>R</i> ₁ = 0.0403, <i>wR</i> ₂ = 0.1158	<i>R</i> ₁ = 0.0943, <i>wR</i> ₂ = 0.2488
Final <i>R</i> indexes [all data]	<i>R</i> ₁ = 0.0411, <i>wR</i> ₂ = 0.1165	<i>R</i> ₁ = 0.1252, <i>wR</i> ₂ = 0.2674
CCDC number	2094453	2094241

Supporting figures

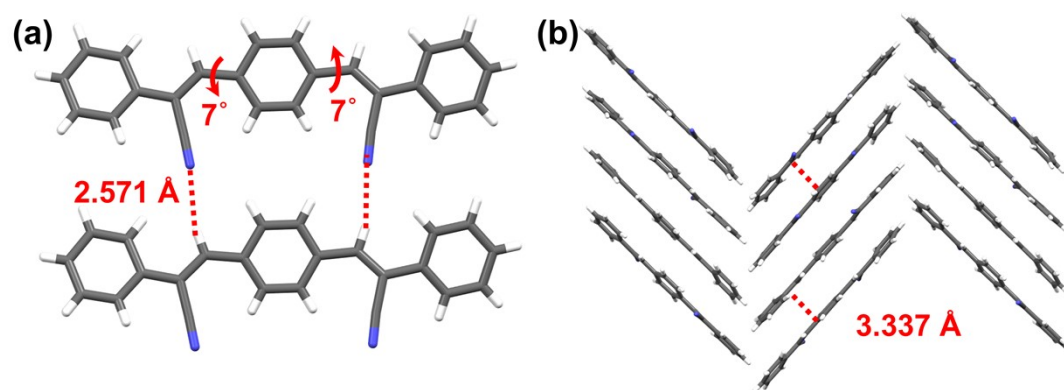


Figure S1 The hydrogen bond and $\pi \cdots \pi$ interactions in CNDSB single crystal structure.

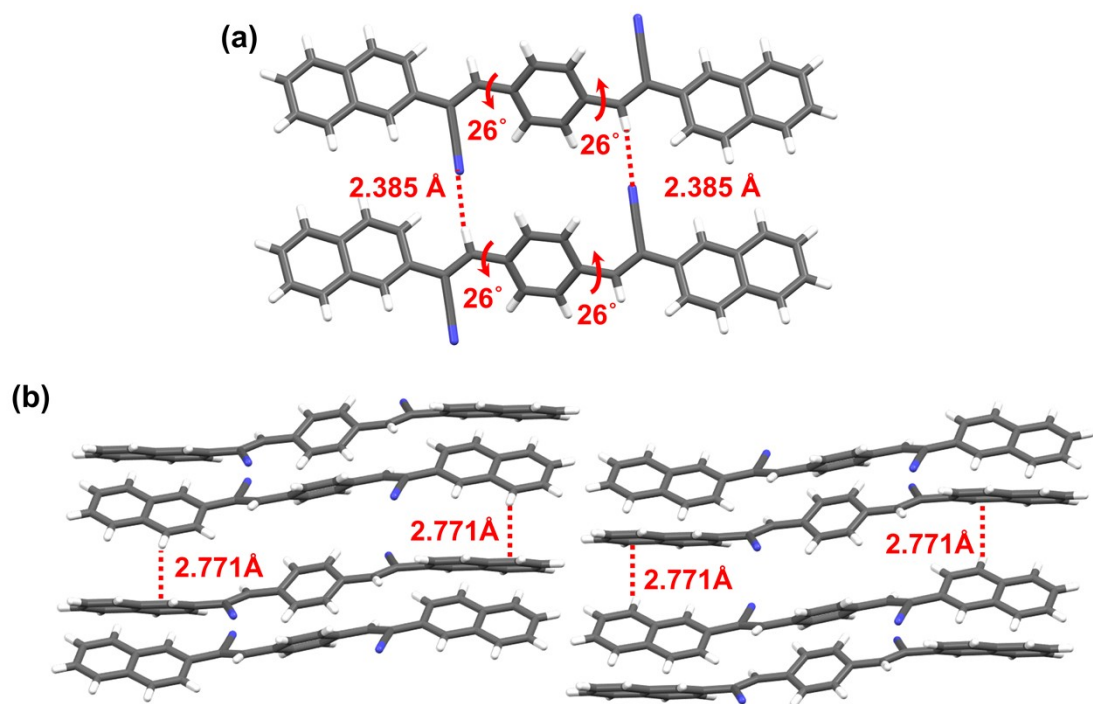


Figure S2 The hydrogen bond and C-H \cdots π interactions in PBNA single crystal structure.

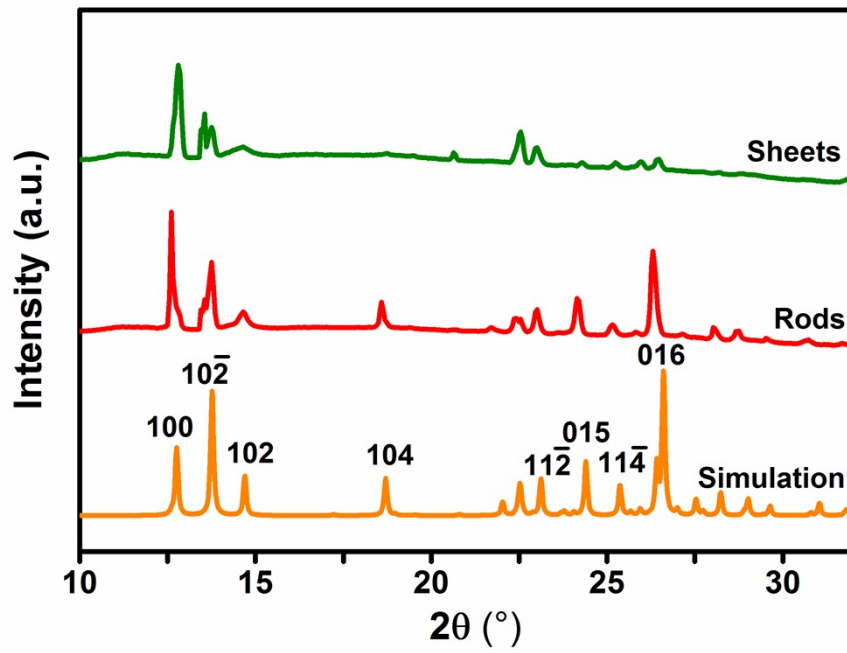


Figure S3 The PXRD measurements of rods and sheets versus simulation for NBTA crystals.

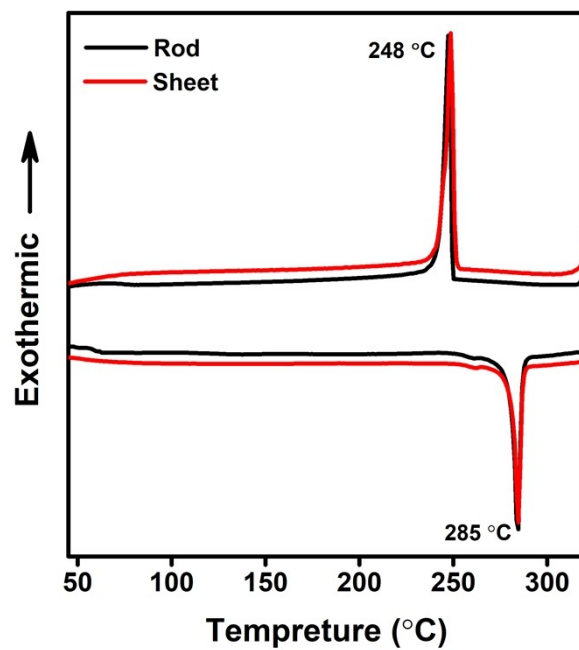


Figure S4 The DSC curves of rods and sheets. They possess the same melting temperatures of 285 °C, indicating the same energy and stability.

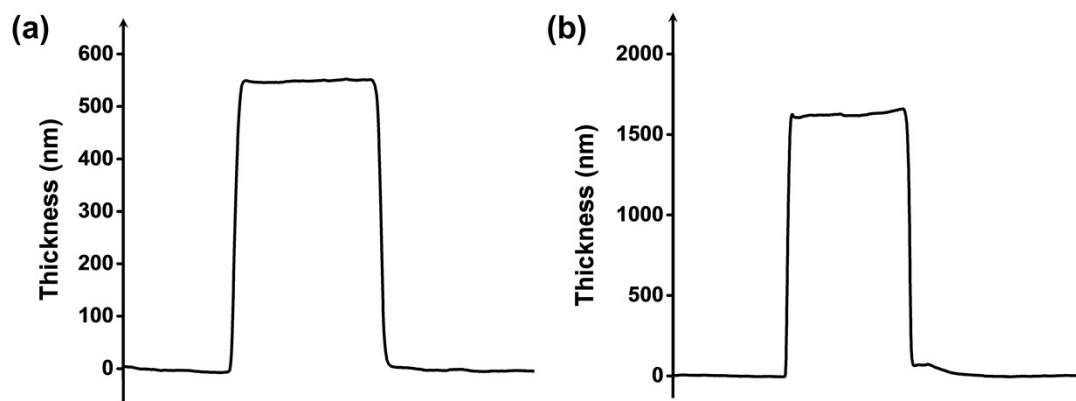


Figure S5 The crystal thickness of NBTA sheets under different growth temperature tested by the surface profiler.

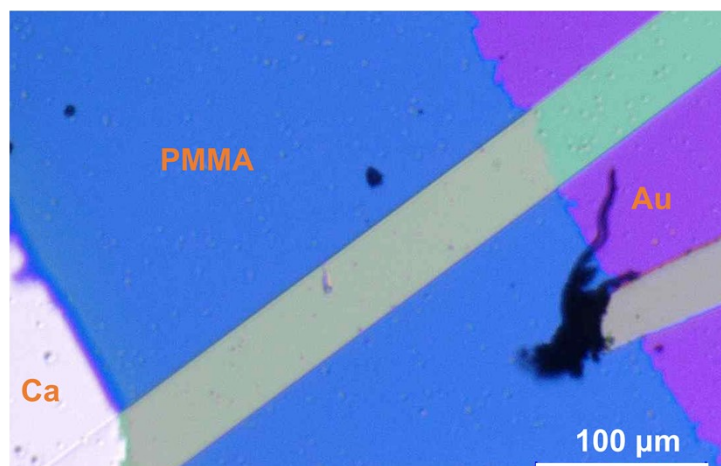


Figure S6 The photograph of organic field-effect transistor device for NBTA single crystal. (Note: The PMMA was used as dielectric modification layer, where the Ca and Au were served as electrodes, and the MoO₃ and CsF were used as hole and electron buffer layers, respectively.)

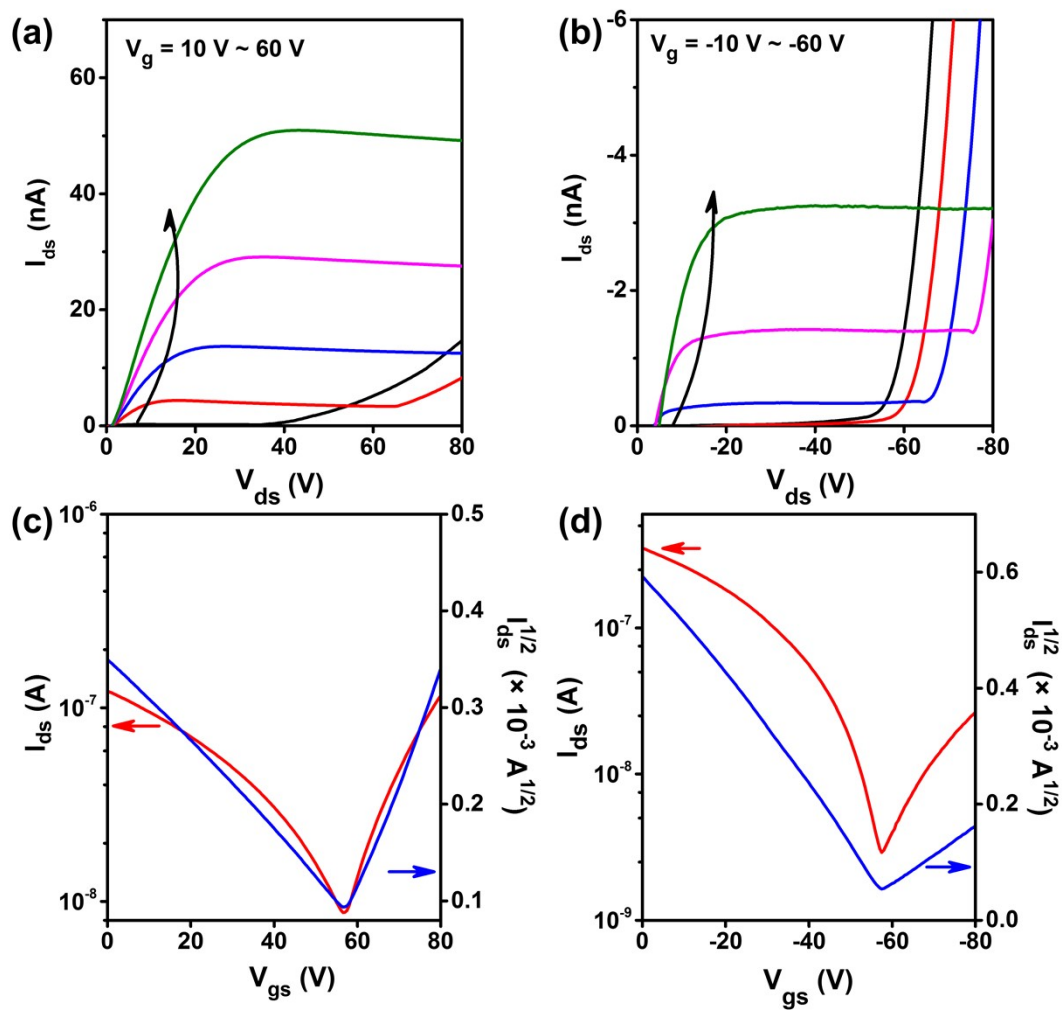


Figure S7 The typical output (a, b) and transfer (c, d) curves under n- and p-channel operation modes in the organic field-effect transistor devices based on NBTA single crystal.